Mn_2Al-LDH- and Co_2Al-LDH-stearate as photodegradants for LDPE film

Bheki Magagula, Nontete Nhlapo and Walter W Focke*

Institute of Applied Materials, Department of Chemical Engineering, University of Pretoria, Lynnwood Road, Pretoria 0002, South Africa

Abstract

The layered double hydroxides (LDH) Mn_2Al-LDH-stearate and Co_2Al-LDH-stearate were prepared by a surfactant-assisted intercalation of the corresponding precursor LDH-CO_3 forms. These compounds were evaluated as potential photodegradant additives in low density polyethylene films with a thickness of ca. 40 mm. They were incorporated into blown polyethylene films via a 10% masterbatch. The films were subjected to accelerated ageing in a QUV weatherometer. The machine was fitted with A320 lamps and operated on a dry cycle at 63 °C and an irradiance of 0.67 W/m^2. It was found that 100 h of QUV exposure was sufficient to cause mechanical embrittlement of films containing as little as 0.1% of either active.

Key words: Layered double hydroxide, cobalt, manganese, photodegradation, polyethylene

* Corresponding author: Tel.: +27833266549, Fax: +27124202516,
e-mail: walter.focke@up.ac.za

1. Introduction

Conventional polymer articles such as plastic film bags are fairly resistant to environmental degradation. They have a high surface-to-volume ratio and may also be brightly colored. Littering of such bags presents a substantial "visual" pollution problem. According to Guilet [1] the most effective way to deal with this litter problem is to reduce the "life time" of the littered objects. Photodegradation can aid rapid disintegration of polymers into a powdery residue with a much-reduced visual impact [2-4]. Further abiotic degradation of such polyethylene can reduce molecular mass to levels where the material becomes susceptible to biodegradation [3, 5-8]. Prodegradant additives are used to enhance such oxo-biodegradation of polyolefins [4, 7-13]. Transition metal carboxylates are particularly suitable for this purpose [12, 14, 15]. Products based on cobalt [16-20] iron [21-23], manganese [3, 24] and cerium [25] have been commercialized. It is believed that they function as catalytic hydroperoxide decomposition agents via the cycle of redox reactions shown in Scheme I [26].

$$\mathrm{ROOH + M^{2+} \rightarrow RO^{\bullet} + HO^{-} + M^{3+}}$$

$$\mathrm{ROOH + M^{3+} \rightarrow ROO^{\bullet} + H^{+} + M^{2+}}$$

$$\text{Overall:} \quad \mathrm{2ROOH \rightarrow RO^{\bullet} + ROO^{\bullet} + H_2O}$$

Scheme I. The cycle of redox reactions whereby transition metal ions catalyze the decomposition of hydroperoxides to produce alkoxy and peroxy radicals [26].

1.1. *Polymer nanoclay composites*

The preparation and properties of polymer nanoclay composites is currently very actively researched. There is special interest in organically modified clays that are amenable to delamination or even exfoliation in the polymer matrix [27-29]. The reason is that such highly dispersed clay platelets impart attractive physical properties at relatively low loadings. Increased stiffness and strength, fire resistance and good gas barrier properties can be achieved without impacting negatively on other desirable polymer characteristics. Most studies have considered organically modified smectite-based clays but reports dealing with anionic clays, i.e. those based on layered double hydroxides (LDH) are on the increase [30-33]. Nanoparticle incorporation into

polymers has been explored for purposes of both photostabilization [34] and photodegradation [35]. Interestingly it was found that conventional smectite clay-based polyethylene nanocomposite showed enhanced susceptibility to photo-degradation [36]. The objective of this study is to explore the photostability of polyethylene nanocomposites containing stearate intercalated layered double hydroxides (LDH).

LDH feature the general chemical formula ($[M^{II}_{1-x}M^{III}_{x}(OH)_2]^{x+}A^{y-}_{x/y}.z\,H_2O$) with M^{II} = Mg, Zn, Fe, Co, Ni, Cu; M^{III} = Al, Fe, Cr, and A = any suitable counterbalancing anion [37]. Carbonate is the most common anion encountered in LDH materials. The structure of LDH compounds consists of trioctahedral metal hydroxide sheets that alternate with interlayers containing anions and water. The brucite-like sheets have a net positive charge per formula unit owing to isomorphic substitution of some of the divalent cations by the trivalent ones. This net positive charge is balanced by an equal negative charge from the interlayer anions. Water molecules also occupy the interlayer space. In this communication the following short hand notation is used to indicate composition: $M^{II}_{n}M^{III}-LDH-A$ where n = 1/x -1. Several recent LDH reviews are relevant to polymer applications [30, 31, 38-40].

Owing to the flexibility with respect to composition a wide range of LDH materials can be tailored for specific applications such as basic catalysts, as precursors for mixed metal oxide catalysts, and as absorbents. Polymer additive applications include heat retention additives for horticultural films [31], flame retardants [33, 44], chloride scavenger in polyolefins [45], heat stabilizer for PVC [46-48], photo- and heat stabilizing agent for organic pigments, etc.

Reichle [50] pioneered the synthesis of Co_2Al-LDH-CO_3 and Mn_3Al-LDH-CO_3. Several authors discussed the synthesis and characterization procedures for manganese-based LDH [51-54] and cobalt-based LDH [54-67]. Ulibarri et al. (1991) [55] drew attention to the fact that the divalent cobalt tends to oxidize to a higher oxidation state during the conventional synthesis process. Herrero et al. [67] indicate that this can largely be circumvented by proper pH control and by reducing the ageing time, e.g. by microwave heating. Miyata and Kumura [68] first reported the intercalation of α,ω-dicarboxylic acids in hydrotalcite. Aisawa et al. [53] prepared dicarboxylic acid intercalated Mn_nAl-LDH and Prévot et al. [64] prepared Co_2Al-LDH-benzoate. To the best of our knowledge, the present study is the first that reports on stearate intercalated manganese- and cobalt-based LDH.

Carlino [69] reviewed intercalation methods for carboxylic acids and also the mechanisms involved. Intercalation of organic anions depends on the extent of intermolecular interactions more so than on the valence or size of the guest molecules [70]. In aqueous solution hydrophobic interactions between the guest molecules provides a driving force that operates in addition to the electrostatic interactions. Long chain aliphatic carboxylate favor a bilayer structure with the intercalation of carboxylate significantly exceeding the anion exchange capacity (AEC) [70].

1.2 *Polymer photodegradation*

Rabek [71] reviewed both photodegradation mechanisms and experimental techniques for monitoring polymer degradation. Ozawa et al. [15] and Audoin et al. [72], among others, have proposed comprehensive kinetic models describing the degradation process. Unfortunately, the heterogeneous nature of photodegradation complicates the determination of the applicable rate constants in the weathering of bulk polymer samples [73-75]. The progression of polymer degradation can be followed various chemical, physical and mechanical methods [24, 71] including differential scanning calorimetry (DSC), thermogravimetric analysis (TG) [20], gel permeation chromatography (GPC) [76, 77], X-ray photo-electron spectroscopy (XPS), chemiluminescence (CL) [78], Fourier transform infrared spectroscopy (FTIR) [26, 79], oxygen uptake [80], CO_2 evolution studies [81, 82] and mechanical testing [24, 26, 83]. FTIR is widely used to follow the time evolution of changes in the functional groups present [79]. Accelerated testing is essential for testing new additives as it shortens the product design-development-production cycle [75]. Therefore this study employed QUV weathering and followed the degradation of the films containing LDH-based photodegradants by FTIR. The apparent degree of degradation was characterized using a Carbonyl Index (CI) defined as the ratio of the maximum absorbance in the carbonyl band near 1720 cm^{-1} to that at 720 cm^{-1}

$$CI = \frac{A_{1720}}{A_{720}}$$

The reference band is due to -CH_2- in-phase rocking vibrations of straight chain methylene sequences containing seven or more carbons. In solid samples, this band appears as a doublet in the infrared spectrum.

2. Experimental

2.1 *Materials*

Chemically pure (CP) grade reagents were used throughout. Aluminium sulphate-18 hydrate 98%, manganese(II) sulphate monohydrate 98%, sodium hydroxide 98%, acetone 99.5%, ammonia 25% solution were all obtained from Saarchem. Other chemicals used and their suppliers were: Sodium carbonate 99% (Dana Chemicals), aluminum nitrate 98.5% (Merck), cobalt(II) nitrate 99% (Radchem), Tween 60 (Sigma Aldrich), and stearic acid (Croda). Two different grades of low density polyethylene (LDPE) were used. Polyethylene powder (grade LT 019/08 ex Sasol, MFI = 20.5 g/10 min; density = 0.919 g/cm^3) was used to prepare masterbatches by extrusion compounding. Films were blown using resin grade LT 660 ex Sasol, MFI = 2 g/10 min; density = 0.923 g/cm^3.

2.2 *Preparation of Mn_2Al-LDH-CO_3 and Co_2Al-LDH-CO_3*

Mn_2Al-LDH-CO_3 and Co_2Al-LDH-CO_3 were synthesized Reichle's [50] coprecipitation method at low supersaturation. The metal salts solution was prepared as follows: 134.99 g (0.4051mol) aluminum sulphate and 137.15 g (0.8114 mol) manganese(II) sulphate were dissolved into homogenous solution in a beaker. Sodium hydroxide and sodium carbonate solution was prepared in a separate beaker by dissolving 113.52 g (2.840 mol) sodium hydroxide and 64.40 g (0.6076 mol) sodium carbonate in enough distilled water. The two solutions were mixed together slowly in 1000 ml beaker under vigorous stirring. The pH of the mixture was kept constant at pH=10 throughout the reaction by careful adjustment of the solution flow rates. The resulting gel was left to stir at room temperature for 18 hours. The product was recovered by

centrifugation, washed four times with distilled water and once with acetone. The product was dried at room temperature.

The same procedure as above was used to prepare Co_2Al-LDH-CO_3 using: aluminum nitrate 109.53 g (0.3287 mol), cobalt(II) nitrate 191.62 g (0.6584 mol), sodium hydroxide 92.1 g (2.3025 mol) and sodium carbonate 52.259 g (0.493 mol).

2.3 *Stearate intercalation*

The stearic acid intercalated products were prepared according to a procedure described by Nhlapo *et al.* [84]. Approximately 100 g Mn_2Al-LDH-CO_3 or Co_2Al-LDH-CO_3, 47 g stearic acid and 40 g surfactant (Tween 60) were suspended in 2000 ml distilled water. The reaction temperature was maintained at 80°C for 8 hours and then allowed to cool down overnight. NH_4OH was added to maintain pH ≈ 10. This heating cooling cycle was repeated four times. Two additional portions of stearic acid (47 g) were added on the second and third cycles so that the overall total amount of 140 g was reached. In the last cycle the mixture was simply allowed to stir for 8 hours without stearic acid addition. The mixture was allowed to cool down slowly to ambient. The solids were recovered by centrifugation, washed once with distilled water, four times with ethanol and once with acetone. The final product, stearate intercalated LDH, was allowed to dry at room temperature.

2.4 *Processing*

Masterbatches were prepared by first mixing the polyethylene and additive powders together. Masterbatches containing 10 % of the intercalated LDH additives were prepared using a 25 mm, 30 L/D Rapra CTM single screw extruder. The screw speed was 40 rpm and the temperature profile: 90 °C/180 °C/180 °C/180 °C. Antioxidant masterbatches (20 % active content) were compounded at 20 kg/h using a 40 mm, 42 L/D Berstorff model EV 40 co-rotating

twin screw extruder using a flat temperature profile set at 180°C. Two vents allowed water vapor to escape from the polymer melt. In both cases LDPE grade LT 019/08 was used as carrier resin. The exiting polymer strands were cooled using a water bath and granulated using a LabTech Engineering model LSC 108 pelletizer. Table 1 lists the three different types of antioxidant that were used in this study. The masterbatch was added, at various let-down levels, to the film grade (LT 660) low density polyethylene resin. Film samples (thickness ca. 36 μm) were blown on a LabTech Engineering Model LF-400 COEX 3-layer laboratory film blower film blower using only one of the two extruders. The screw speed was set at 40 rpm and a flat temperature profiles (180 °C) was used.

<Table 1>

2.5 *Artificial weathering*

The film samples were subjected to artificial weathering in a QUV accelerated weathering tester fitted with A340 UV lamps. A dry cycle was used with the temperature set at 63 °C and the irradiance at 0.67 W/m^2. The rate of polymer oxidation was followed by IR spectroscopy by measuring the growth of the carbonyl peak near 1720 cm^{-1}. A Carbonyl Index, defined as the ratio of this absorption to that at 720 cm^{-1}, was used to quantify the degradation progress.

2.6 *Characterization*

The LDH carbonates and stearate intercalated samples were analyzed using SEM, FTIR spectroscopy, TGA/DTA and XRD. Small amounts of the powder product or LDH-CO_3 precursor were placed onto carbon tape on a metal sample holder. Excess powder was removed using a compressed air blast. Samples were coated five times with gold using Scanning Electron Microscope (SEM) autocoating unit E5200 (Polaron equipment LTD) under argon gas. Gold coated particles were viewed on a JEOL 840 SEM scanning electron microscope under low magnification.

A Mettler Toledo A851 simultaneous TGA/SDTA machine was used for differential thermal analysis (DTA) and thermo-gravimetric (TG) analysis. Powder or film samples (ca. 10 mg) were placed in open 70 μl alumina pan and heated from 25°C to 900°C at a scan rate of

10°C/min in air flowing at 50 ml/min. The oxidation onset temperatures (OOT) for films were determined using the same conditions.

Infrared spectra were recorded on a Perkin Elmer Spectrum RX I FT-IR system. The films were mounted on card board frames and tested in the neat and artificially weathered states. The KBr method was used for powder samples. The pressed pellets contained approximately 2 mg of sample and 100 mg of KBr. Data obtained from 32 scans recorded at a resolution of 2 cm^{-1} were averaged and background-corrected using a pure KBr pellet.

XRD analysis was carried out by on a PANalytical X-pert Pro powder diffractometer with variable divergence- and receiving slits and an X'celerator detector using Fe filtered Co K-alpha radiation (0.17901 nm). X'Pert High Score Plus software was used for phase identification.

3. Results and discussion

3.1 *Characterization of the LDH additives*

The SEM picture of the Mn_2Al-LDH-stearate particles is shown in Figure 1. Their shape approximates to high aspect ratio flakes and they are several μm across.

<Fig. 1>

<Fig. 2>

Figure 2 shows the XRD results for the precursor Co_2Al-LDH-CO_3 and the intercalated product Mn_2Al-LDH-stearate. The corresponding XRD spectra for Mn_2Al-LDH-CO_3 and Co_2Al-LDH-stearate are not shown as they appear similar. The sharp patterns, for the precursor and the intercalated clay, confirm that highly crystalline products were obtained. The first peak is due to the 003 reflection and the shift in its position indicates that the d-spacing increased from 0.76 nm to 4.7 nm for both products. This is consistent with double layer intercalation of the stearic acid [84].

<Fig. 3>

The thermogravimetric trace for Mn_2Al-LDH-CO_3 and Mn_2Al-LDH-stearate obtained in an air atmosphere is shown in Figure 3. The mass loss of Mn_2Al-LDH-CO_3 mimics that for the

conventional Mg_2Al-LDH-CO_3 form. Mass loss of the carbonates proceeds stepwise with three distinct but overlapping peaks in the DTG trace. These events are commonly attributed to the loss of interlayer water, dehydroxylation and a combination dehydroxylation-decarbonation reaction respectively [50, 84]:

$[Mn_2Al(OH)_6]\ (CO_3)_{1/2}\cdot 1.5H_2O \rightarrow [Mn_2Al\ (OH)_6](CO_3)_{1/2} \rightarrow 2\ MnO + 1/2\ Al_2O_3$

Scheme II: Mass loss sequence for Mn_2Al-LDH-CO_3

For Mn_2Al-LDH-CO_3 the expected and experimentally observed values for the TG residues after the final degradation step (measured at 900°C) are 65.2 % and 68.7 % respectively. The corresponding TG residue values for Co_2Al-LDH-CO_3 are 66.1 % and 67.6 % respectively. The small discrepancy could be due to the presence of impurities or a lower degree of hydration than indicated for the products. Decomposition of the stearate intercalated LDH samples follows a similar pattern.

The degree of intercalation was estimated from the mass loss values determined at 150°C (dehydrated state) and 900°C (only oxides present) [84]. Stearate intercalation levels equivalent to 221 % and 151 % of the theoretical anion exchange capacities of the Mn_2Al-LDH-CO_3 and Co_2Al-LDH-CO_3 clays respectively, were obtained by this calculation. Stated in another way, the organic (stearate) content on a dry clay basis amounted to 70.6 % and 62.8 % for the two additives. This should be compared to the ca. 94 % by mass organic content of the corresponding metal (III) stearate soaps. Clearly this means that the intercalated double hydroxides contain higher levels of the catalytically active inorganic moiety than the corresponding stearate soaps.

<Fig. 4>

Figure 4 compares the FTIR spectra of Mn_2Al-LDH-stearate with those for Mn_2Al-LDH-CO_3 and stearic acid. Kannan et al. [57] and Kloprogge and Frost [60, 61] report detailed band assignments for the carbonate forms. The broad band in the region 3200 - 3700 cm^{-1} is observed in all the LDH compounds. It is attributed to O–H stretching vibrations of the octahedral layer hydroxides and intercalated water molecules. The characteristic peak at 420 cm^{-1} (O–M–O bending mode) and those at 530 and 615 (M–O stretching modes) indicate an intact LDH sheet

structure. The carbonate peak located at ca. 1420 cm^{-1} is well developed in LDH-CO_3. Its presence in the LDH-stearate indicates the presence of LDH-CO_3 as an impurity. The triplet peaks observed in the range 2850-2965 cm^{-1} in the LDH-stearates are due to C–H stretching [84]. They confirm intercalation of the alkyl chains of the stearic acid. The carboxylate asymmetric stretching vibrations bands near 1540 cm^{-1} are typical for LDH-stearates. The ν(C=O) stretching vibration at 1700 cm^{-1}, observed for stearic acid, is absent in the stearate intercalated products.

3.2 *Accelerated artificial weathering*

The blown films containing the two additives were completely translucent indicating that they were probably dispersed at the nanoscale level. Figures 5 to 9 detail the evolution of degradation in the polymer films as a function of QUV exposure time. Figure 5 illustrates the growth of the carbonyl peak at 1710 cm^{-1} with increasing exposure time. This indicates progressive oxidation of the base polymer. Inspection by poking with a blunt needle revealed that even the samples made using 1% masterbatch, i.e. containing only 0.1% of either of the prodegradants, were mechanically embrittled after only 100 h of artificial weathering.

<Fig. 5>

<Fig. 6>

<Fig. 7>

Figures 6 and 7 shows the effect of additive concentration and exposure time on the carbonyl index. CI increases to a value of about 0.6 for the virgin LDPE film after 250 h of QUV exposure. CI rises much more rapidly for the samples containing the additives and exceeds this value in an exposure time below 50 h. Interestingly the most significant increase is between the virgin polymer and the film containing 0.10 % LDH. Increasing the additive content above this level up to 0.48 %does lead to faster UV degradation but the difference is almost marginal.

<Fig. 8>

<Fig. 9>

Figures 8 and Figure 9 show the effect of adding antioxidants using loading of 0.2 % for both the LDH and the stabilizer. The nature of the antioxidants appears irrelevant with Mn_2Al-LDH-stearate as additive as there is little difference in performance. All oxidants cause a slight decrease in the observed CI values. The results for Co_2Al-LDH-stearate as additive were similar

except that in this case the amine-based antioxidant Orox PK appears to have had almost no retarding effect on CI growth.

3.3 *Oxidative stability at processing temperatures*

The oxidation onset temperature (OOT) corresponds to the onset temperature (T_{onset}) of the exothermic oxidation reaction in an oxygen containing atmosphere [85]. OOT provides a provisional indication of the oxidative stability of a polymer at temperatures relevant to processing conditions. In this study thermal stability in the presence of different antioxidant was determined in air. The results are summarized in Figure 10 for the situation where the additives were present at a concentration of 0.20 %. The OOT for the neat LDPE was determined as 227.6 °C. Adding Naugard P or Orox PK caused a marginal increase but adding 0.20 % of the phenolic antioxidant Anox 20 raised OOT to 262 °C. Adding the LDH additives to the neat LDPE caused a significant lowering of OOT values. When antioxidants were also added, the OOT values improved with effectiveness increasing in the series Naugard P < Orox PK < Anox 20. Co_2Al-LDH-stearate on its own caused the greatest drop in OOT. However, the antioxidants were also more effective with this additive compared to the manganese-based LDH. In fact, both Orox PK and Anox 20 showed a synergistic interaction with Co_2Al-LDH-stearate: The measured OOT values were higher than was the case when only the antioxidant was present.

<Fig 10>

$$RH \xrightarrow{\tau,\Delta,h\nu} R^{\bullet} \xrightarrow{O_2} ROO^{\bullet} \xrightarrow{RH} R^{\bullet} + ROOH$$

$$ROOH \xrightarrow{\Delta,h\nu} RO^{\bullet} + {}^{\bullet}OH$$

Scheme III. Simplified reaction scheme for the auto-oxidation of polymers

Scheme III shows, in highly simplified form, the cascade of reactions responsible for oxidative degradation of a polymer such as LDPE. A free radical may form on the polymer (RH) due to the effects of mechanical stress, heat or UV radiation. The free radical rapidly combines with available oxygen to form a peroxy radical. This subsequently abstracts a labile hydrogen from a (nearby) polymer chain, regenerating the original chain free radical and resulting in a hydroperoxide. Under the influence of heat or UV the latter cleaves to form two additional free radicals. This chain reaction causes rapid proliferation of free radicals that ultimately results in polymer chain scission taking place that leads to a loss of mechanical and other desirable polymer properties.

Comparing Scheme I with Scheme III shows that the metal catalytic cycle actual halves the number of free radicals that can potentially be generated by the decomposition of the hydroperoxides. So, in effect, the action of the metal ions is akin to that performed by a secondary antioxidant. The reason why they nevertheless accelerate the auto-oxidation of polymers is attributed to the fact that they greatly accelerate the rate of hydroperoxide decomposition. Nevertheless, it is conceivable that the presence of a suitable primary antioxidant, they will actually aid process stabilization. The OOT results obtained with the phenolic or amine antioxidants, i.e. Anox 20 and Orox PK respectively, in conjunction with Co_2Al-LDH-stearate support this hypothesis. The practical implication is that the processing stability of photodegradant-containing LDPE can be maintained in the presence of a suitable antioxidant. Actually, La Mantia and Gardette [86] previously found that photo-oxidized polyethylene film can be reprocessed. They also found that the recycled film properties were significantly improved compared to those of films before recycling.

4. Conclusions

Mn_2Al-LDH-stearate and Co_2Al-LDH-stearate were successfully prepared from the corresponding carbonate forms using the surfactant-mediated intercalation method. These

additives were incorporated into thin LDPE films. Nearly clear polyethylene films are obtained at low dosage levels of this additive. The rate of photodegradation was followed as a function of QUV exposure time. It was found that both additives are effective UV photodegradants in QUV accelerated weathering tests. Oxidation onset temperatures obtained with a phenolic and an amine-based antioxidant, suggest that the processing stability of the polyethylene can be maintained despite the presence of such photodegradants.

Acknowledgements

Financial support for this research, from the Institutional Research Development Programme (IRDP), the South African Cooperation Fund for Scientific and Technological Developments (NEPAD) and the THRIP program of the Department of Trade and Industry and the National Research Foundation of South Africa, Evergreen (Pty) Ltd as well as Xyris Technology CC, is gratefully acknowledged.

5. References

1. Guilet JE. In: Scott G, editor. Degradable polymers: Principles and applications, 2nd Ed. London: Kluwer, 2003.
2. Gilead D. Photodegradable films for agriculture, Pol Degrad Stab 1990;29: 65 -71.
3. Jakubowicz I. Evaluation of degradability of biodegradable polyethylene (PE), Polym Degrad Stab 2003;80: 39-43.
4. Wiles DM, Scott G. Polyolefins with controlled environmental degradability, Polym Degrad Stab 2006;91: 1581-1592.
5. Albertsson AC, Barenstedt C, Karlsson S, Lindburg T. Degradation product pattern and morphology changes as means to differentiate abiotically and biotically aged degradable polyethylene Polymer 1995;36: 3075-3083.
6. Weiland M, Daro A, David C. Biodegradation of thermally oxidized polyethylene, Polym Degrad Stab 1995;48: 275-289.
7. Chiellini E, Corti A, Swift G. Biodegradation of thermally-oxidized, fragmented low-density polyethylenes, Polym Degrad Stab 2003;81: 341-351.
8. Hasan F, Shah AA, Hameed A, Ahmed S. Synergistic effect of photo and chemical treatment on the rate of biodegradation of low density polyethylene by Fusarium sp AF4, J Appl Polym Sci 2007;105: 1466-1470.
9. Albertsson A-C, Andersson SO, Karlsson S. The mechanism of biodegradation of polyethylene Polym Degrad Stab 1987;18: 73-87.
10. Albertsson A-C, Karlsson S. Three stages in degradation of polymers – polyethylene as a model substance, J Appl Polym Sci 1988;35: 1289-1302.
11. Albertsson A-C, Barenstedt C, Karlsson S. Susceptibility of enhanced environmentally degradable polyethylene to thermal and photo-oxidation. Polym Degrad Stab 1992;37(2): 163-171.
12. Sipinen AJ, Rutherford DR. A study of the oxidative degradation of polyolefins, Proc Am Chem Soc 1992;67: 185-187.

13. Hakkarainen M, Albertsson A-C. Environmental degradation of polyethylene, Adv Polym Sci 2004;169: 177-199.
14. Potts JE, Cornell SW, Sracic AM. Environmentally degradable ethylene polymeric compositions, US Pat 3935141, 1976.
15. Ozawa Z, Kurisu N, Nagashima K, Nakano K. Effect of transition metal stearates on the photodegradation of polyethylene, J Appl Pol Sci 1979;23: 3583-3590.
16. Roy PK, Sureka P, Rajagopal C, Chatterjee SN, Choudhary V. Effect of benzil and cobalt stearate on the ageing of low-density polyethylene films, Polym Degrad Stab 2005;90: 577-585.
17. Roy PK, Sureka P, Rajagopal C, Choudhary V. Study on the degradation of low-density polyethylene in the presence of cobalt stearate and benzyl, J Appl Polym Sci 2006;99: 236-243.
18. Roy PK, Sureka P, Rajagopal C, Choudhary V. Effect of cobalt carboxylates on the photo-oxidative degradation of polyethylene Part I Polym Degrad Stab 2006;91: 1980-1988.
19. Roy PK, Sureka P, Rajagopal C, Chatterjee SN, Choudhary V. Accelerated aging of LDPE films containing cobalt complexes as prooxidants, Polym Degrad Stab 2006;91: 1791-1799.
20. Roy PK, Sureka P, Rajagopal C, Choudhary V. Thermal degradation studies of LDPE containing cobalt stearate as pro-oxidant, eXPRESS Polymer Letters 2007;1: 208-216.
21. Al-Malaika S, Marogi AM, Scott G. Mechanisms of antioxidant action: Time-controlled photoantioxidants for polyethylene based on soluble iron compounds, J Appl Polym Sci 1986;31: 685-698.
22. Ferguson GM, Hood M, Abbott K. Photodegradable high density polyethylene-based shopping bags - environmental hazard or blessing?, Polym Int 1991;28: 35-40.
23. David C, Trojan M, Daro A. Photodegradation of polyethylene: comparison of various photo-initiators in natural weathering conditions, Polym Degrad Stab 1992;37: 233-245.
24. Khabbaz F, Albertson A-C. Rapid test methods for analyzing degradable polyolefins with a pro-oxidant system J Appl Polym Sci 2001;79: 2309-2316.
25. Lin Y. Study of photooxidative degradation of LDPE film containing cerium carboxylate photosensitizer. J Appl Polym Sci 1997;63: 811-818.
26. Amin MU, Scott G. Photo-initiated oxidation of polyethylene effect of photo-sensitizers, Eur Polym J 1974;10: 1019-1028.
27. LeBaron PC, Wang Z, Pinnavaia TJ, Polymer-layered silicate nanocomposites: an overview, Appl Clay Sci 1999;15:11-29.
28. Ray SS, Okamoto M. Polymer/layered silicate nanocomposites: a review from preparation to processing, Prog Polym Sci 2003;28: 1539-1641.
29. Utracki LA, Sepehr M, Boccaleri E. Synthetic, layered nanoparticles for polymeric nanocomposites (PNCs), Polym Adv Technol 2007;18: 1-37.
30. Leroux F, Besse J-P. Polymer interleaved layered double hydroxide: a new emerging class of nanocomposites, Chem Mater 2001;13: 3507-3515.
31. Evans DG, Duan X. Preparation of layered double hydroxides and their applications as additives in polymers, as precursors to magnetic materials and in biology and medicine, Chem Commun 2006: 485-496.
32. Qiu L, Chen W, Qu B. Morphology and thermal stabilization mechanism of LLDPE/MMT and LLDPE/LDH nanocomposites, Polymer 2006;47: 922-930.
33. Costa FR, Wagenknecht U, Heinrich G. LDPE/Mg-Al layered double hydroxide nanocomposite: Thermal and flammability properties, Polym Degrad Stab 2007;92: 1813-1823.

34. Ammala A , Hill AJ, Meakin P , Pas SJ, Turney TW. Degradation studies of polyolefins incorporating transparent nanoparticulate zinc oxide UV stabilizers, J Nanopart Res 2002;4 : 167-174.
35. Angulo-Sanchez JL, Ortega-Ortiz H, Sanchez-Valdes S. Photodegradation of polyethylene films formulated with a titanium-based photosensitizer and titanium dioxide pigment, J Appl Polym Sci 1994;53: 847-856.
36. Qin H, Zhao C, Zhang S, Chen G, Yang M. Photo-oxidative degradation of polyethylene/montmorillonite nanocomposites, Polym Degrad Stab 2003;81: 497-500.
37. Vaccari A. Preparation and catalytic properties of cationic and anionic clays. Catal Today 1998;41: 53-71.
38. Cavani F, Trifirò F, Vaccari A. Hydrotalcite-type anionic clays: preparation, properties and applications, Catal Today 1991;11: 173-301.
39. Newman SP, Jones W. Synthesis, characterization and layered double hydroxides containing organic guests, New J Chem 1998: 105-115
40. Khan AI, O'Hare D. Intercalation chemistry of layered double hydroxides: recent developments and applications, J Mat Chem 2002;12: 3191-3198.
41. Fischer H. Polymer nanocomposites: from fundamental research to specific applications, Mater Sci Eng, 2003;C23: 763-772.
42. Leroux F, Taviot-Guého C. Fine tuning between organic and inorganic host structure: new trends in layered double hydroxide hybrid assemblies, J Mat Chem 2005;15: 3628-3641.
43. Williams GR, O'Hare D. Towards understanding, control and application of layered double hydroxide chemistry, J Mater Chem 2006;16: 3065-3074.
44. Constantino U, Gallipoli A, Nochetti M, Camino G, Bellucci F, Frache A. New nanocomposites constituted of polyethylene and organically modified ZnAl-hydrotalcites, Polym Degrad Stab 2005;90: 586-590.
45. Meyn M, Beneke K, Lagaly G. Anion-exchange reactions of layered double hydroxides, Inorg Chem 1990;29: 5201-5207.
46. Batenburg LF, Fischer HR, Gielgens LH, Koster TPM, van Gemert MLM, van der Ven L. On the action of hydrotalcite-like clay materials as stabilisers is polyvinylchloride Applied Clay Science 2000;17: 25-34.
47. Lin Y-J, Li D-Q, Evans DG, Duan X, Li D, Lin Y. Modulating effect of Mg-Al-CO_3 layered double hydroxides on the thermal stability of PVC resin, Polym Degrad Stab 2005;88: 286-293.
48. Lin Y, Wang J, Evans DG, Lin D. Layered and intercalated hydrotalcite-like materials as thermal stabilizers in PVC, J Phys Chem Solids 2006;67: 998-1001.
49. Guo S, Evans DG, Li D. Preparation of CI pigment 52:1 anion-pillared layered double hydroxide and the thermo- and photostability of the resulting intercalated material, J Phys Chem Solids 2006;67: 1002-1006.
50. Reichle WT. Synthesis of anionic clay minerals (mixed metal hydroxides, hydrotalcite), Solid State Ionics 1986;22: 135-141.
51. Carrado KA, Kostapapas A, Suib SL. Layered double hydroxides (LDHs), Solid State Ionics, 1988;26: 77-86.
52. Malherbe F, Forano C, Besse JP. First coprecipitation of an LDH containing manganese as the divalent cation J Mater Sci Lett, 1999;18: 1217-1219.
53. Aisawa S, Hirahara H, Uchiyama H, Takahashi S, Narita E Synthesis and thermal decomposition of Mn-Al layered double hydroxides, J Solid State Chem 2002;167: 152-159

54. Kovanda F, Rojka T, Dobešova J, Machovič V, Bezdička P, Obalová L, Jiratová K, Grygar T. Mixed oxides obtained from Co and Mn containing layered double hydroxides: Preparation, characterization, and catalytic properties, J Solid State Chem 2006;179: 812-823.
55. Ulibarri MA, Fernandez JM, Labajos FM, Rives V. Anionic clays with variable valence cations: synthesis and characterization of cobalt aluminum hydroxide carbonate hydrate $[Co_{1-x}Al_x (OH)_2](CO_3)_{x/2}\cdot nH_2O$, Chem Mater 1991;3: 626 – 630.
56. Kannan S, Swamy CS. Synthesis and physicochemical characterization of cobalt aluminium hydrotalcite, J Mater Sci Lett 1992;11: 1585-1587.
57. Kannan S, Velu S, Ramkumar V, Swamy CS. Synthesis and physicochemical properties of cobalt aluminium hydrotalcites, J Mater Sci 1995;30: 1462-1468.
58. Qian M, Zeng C. Synthesis and characterization of Mg-Co catalytic oxide materials for low-temperature N_2O decomposition, J Mater Chem 1997;7 493-499.
59. Ribet S, Tichit D, Coq B, Ducourant B, Morato F. Synthesis and activation of Co-Mg-Al Layered double hydroxides, J Solid State Chem 1999;142 382-392.
60. Kloprogge JT, Frost RL. Fourier transform infrared and Raman spectroscopic study of the local structure of Mg, Ni and Co-hydrotalcites, J Solid State Chem 1999;46 : 506-515.
61. Kloprogge JT, Frost RL. Infrared emission spectroscopy study of the thermal transformation of Mg, Ni and Co hydrotalcite catalysts, Appl Catal A 1999;1814 : 61-74.
62. Xu ZP and Zeng HC. Decomposition process of organic-anion-pillared clays $Co_aMg_bAl(OH)_c(TA)_d\cdot nH_2O$, J. Phys. Chem. B, 2000;104: 10206-10214.
63. Xu, ZP, Zeng HC. Ionic interactions in crystalline growth of CoMgAl-hydrotalcite-like compounds, Chem. Mater. 2001;13: 4555-4563.
64. Prévot V, Casal B, Ruiz-Hitzky E. Intracrystalline alkylation of benzoate ions into layered double hydroxides, J Mater Chem 2001;11: 554-560.
65. Pérez-Ramírez J, Mul G, Kapteijn F, Moulijn JA. A spectroscopic study of the effect of the trivalent cation on the thermal decompositon behaviour of Co-based hydrotalcites, J Mater Sci 2001;11: 2529-2536.
66. Pérez-Ramírez J, Mul G, Kapteijn F, Moulijn JA. *In situ* investigation of the thermal decomposition of Co-Al hydrotalcite in different atmospheres, J Mater Chem 2001;11: 821-830.
67. Herrero M, Benito P, Labajos FM, Rives V. Stabilization of Co^{2+} in layered double hydroxides (LDHs): by microwave-assisted ageing, J Solid State Chem 2007;180: 873-884.
68. Miyata S, Kumura T. Synthesis of new hydrotalcite-like compounds and their physico-chemical properties, Chem Lett 1973: 843-848.
69. Carlino S. The intercalation of carboxylic acids into layered double hydroxides: a critical evaluation and review of different methods, Solid State Ionics 1997;98: 73-84.
70. Kanoh T, Shichi T, Takagi K. Mono- and bilayer equilibria of stearate self-assembly formed in hydrotalcite interlayers by changing the intercalation temperature, Chem Lett 1999: 117-118.
71. Rabek JF. Polymer photodegradation. Mechanism and experimental methods. London: Chapman & Hall, 1995.
72. Audoin L, Gueguen V, Tchaktchi A, Verdu J. “Closed loop” mechanistic schemes for hydrocarbon polymer oxidation, J Polym Sci, Part A: Polym Chem 1995;33: 921-927.
73. Giesse R, De Paoli M-A. Surface and bulk oxidation of low-density polyethylene under UV-irradiation, Polym Degrad Stab 1988;21: 181-187.
74. Gugumus F. Photooxidation of polyethylene films, 1 Experimental kinetics of functional group formation, Angew Makromol Chem 1999;182: 85-109.

75. Pospíšil J, Pilař J, Billingham NC, Marek A, Horák Z, Nešpůrek S. Factors affecting accelerated testing of polymer photostability, Polym Degrad Stab 2006;91: 417-422.
76. Miyagawa E, Tokumitsu K, Tanaka A, Nitta K. Mechanical property and molecular weight distribution changes with photo- and chemical-degradation on LDPE films, Polym Degrad Stab 2007;92: 1948-1956.
77. White JR, S\hyichuk AV. Macromolecular scission and crosslinking rate changes during polyolefin photo-oxidation, Polym Degrad Stab 2007;92: 1161-1168.
78. Koutný M, Václavková T, Matisová-Rychlá L, Rychlý J. Characterization of oxidation progress by chemiluminescence: A study of polyethylene with pro-oxidant additives, Polym Degrad Stab 2008;93(8): 1515-1519.
79. A. Tidjani and R. Arnaud. Photo-oxidation of linear low density polyethylene: A comparison of photoproducts formation under natural and accelerated exposure. Polym. Degrad. Stab. 1993;39: 285-292.
80. Fraïsse F, Kumar A, Commereuc S, Verney V. Photo-oxidation of polymers: Validation of oxygen uptake and relationship with extent of hydroperoxidation, J Appl Polym Sci 2006;99: 2238-2244.
81. Jin C, Christensen PA, Egerton TA, Lawson EJ, White JR. Rapid measurement of polymer photo-degradation by FTIR spectrometry of evolved carbon dioxide, Polym Degrad Stab 2006;91: 1086-1096.
82. Fernando SS, Christensen PA, Egerton TA, White JR. Carbon dioxide evolution and carbonyl group development during photodegradation of polyethylene and polypropylene, Polym Degrad Stab 2007;92: 2163-2172.
83. Miyagawa E, Tokumitsu K, Tanaka A, Nitta K. Mechanical property and molecular weight distribution changes with photo- and chemical-degradation on LDPE films, Polym Degrad Stab 2007;92: 1948-1956.
84. Nhlapo N, Motumi T, Landman E, Verryn SMC, Focke WW. Hydrotalcite: surfactant-assisted fatty acid intercalation of layered double hydroxides, J Mater Sci 2008;43: 1033-1043.
85. Gimzewski E. The relationship between oxidation induction temperatures and times for petroleum products. Thermochim Acta 1992;198:133-140.
86. La Mantia FP, Gardette JL. Improvement of the mechanical properties of photo-oxidized films after recycling, Polym Degrad Stab 2002;75: 1-7.

Figure captions

Figure 1. SEM picture showing the morphology of the Mn_2Al-LDH-stearate particles.

Figure 2. XRD spectrum of Co_2Al-LDH-CO_3 and Mn_2Al-LDH-stearate. The corresponding d-spacings were calculated as 0.76 nm and 4.7 nm. The latter value is consistent with the expected double layer intercalation of stearate in the LDH compound.

Figure 3. TG curves for Mn_2Al-LDH-CO_3 and Mn_2Al-LDH-stearate determined in an air atmosphere at a scan rate of 10°C/min.

Figure 4. FTIR spectra for Mn_2Al-LDH-CO_3, stearic acid and Mn_2Al-LDH-stearate.

Figure 5. Time evolution of the FTIR spectra of QUV weathered films containing 0.10 % Mn_2Al-LDH-stearate.

Figure 6. Effect of Mn_2Al-LDH-stearate concentration on the growth of the carbonyl index during QUV accelerated weathering of polyethylene films.

Figure 7. Effect of Co_2Al-LDH-stearate concentration on the growth of the carbonyl index during QUV accelerated weathering of polyethylene films.

Figure 8. Effect of 0.2 % antioxidant addition on the QUV accelerated weathering of polyethylene films containing 0.2 % Mn_2Al-LDH-stearate.

Figure 9. Effect of 0.2 % antioxidant addition on the QUV accelerated weathering of polyethylene films containing 0.2 % Co_2Al-LDH-stearate.

Figure 10. Effect of antioxidants and LDH-based photodegradants on the thermo-oxidative stability of the polyethylene base resin as characterized by the oxidation onset temperature measured in dynamic scanning mode at 10°C/min in an air atmosphere.

Table 1. Antioxidants

Antioxidant	Supplier	Type	Chemical name
Anox 20	Great Lakes	phenolic	tetrakismethylene (3,5-di-t-butyl-4-hydroxy-hydrocinnamate) methane
Naugard P	Chemtura	phosphite	tris(monononylphenyl)phosphite
Orox PK	Orchem	amine	polymerized 2,2,4-trimethyl-1,2-dihydroquinoline

Figure 1

Click here to download high resolution image

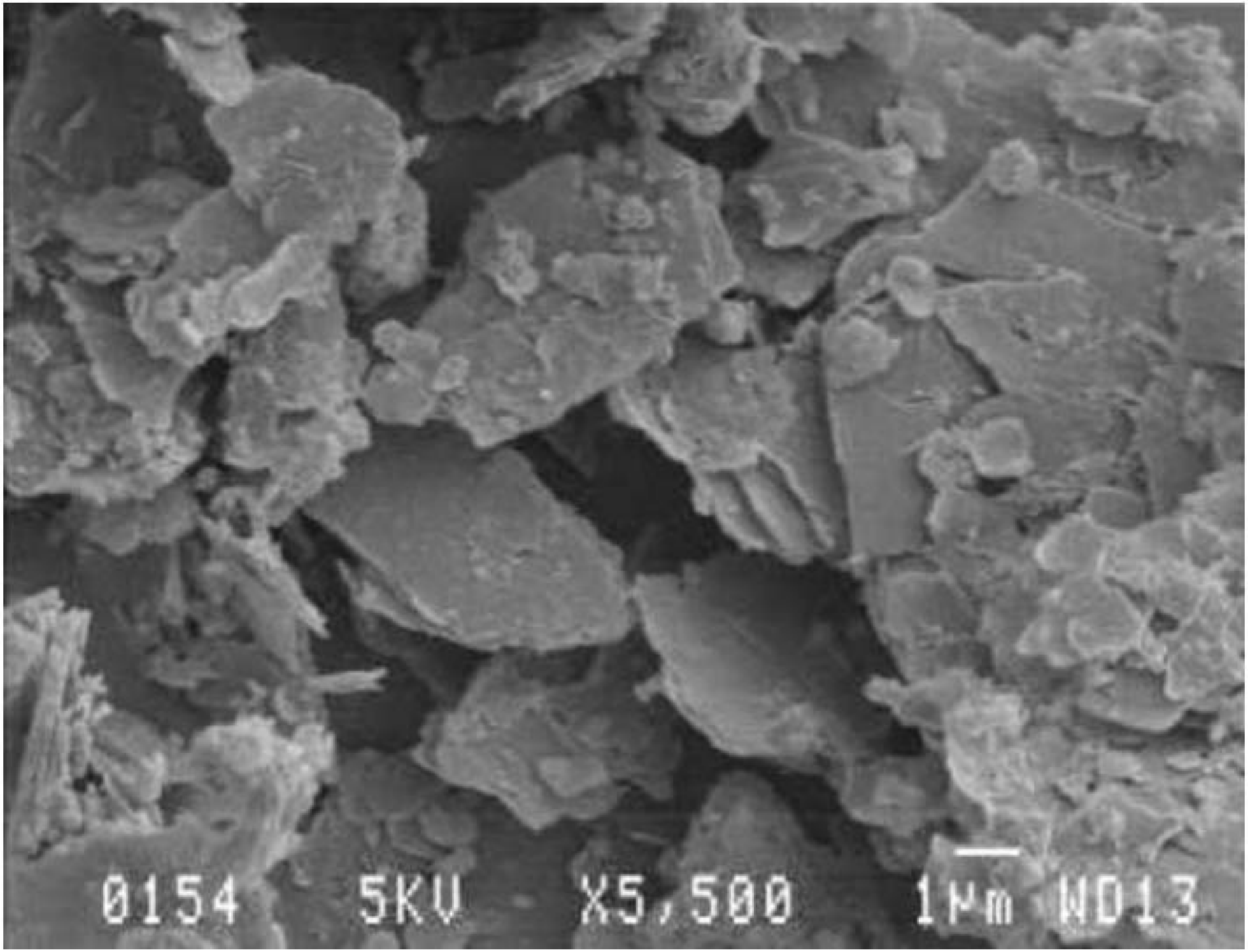

Figure 2

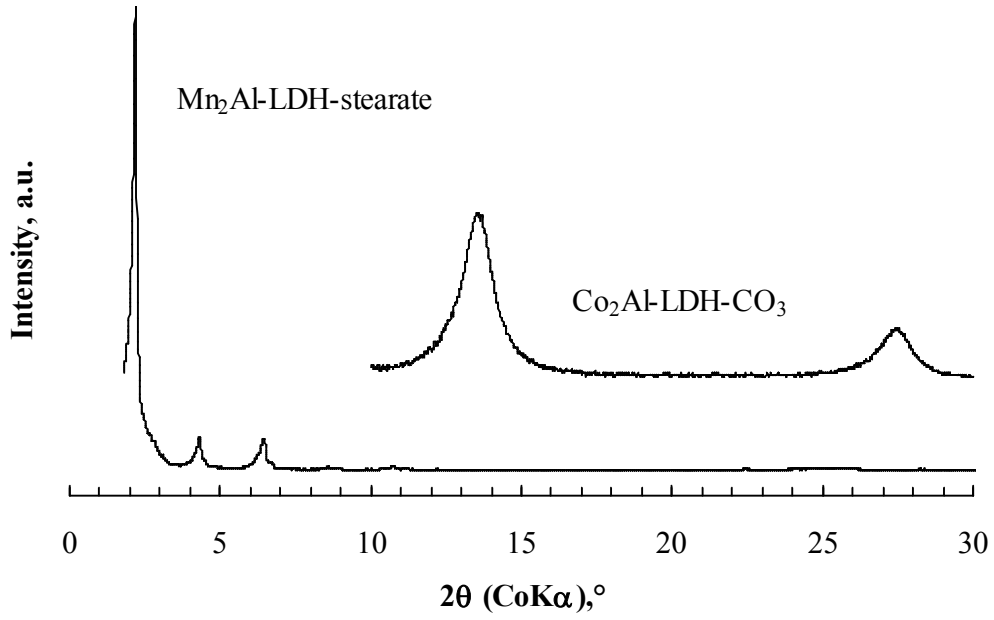
Mn2Al-LDH-stearate
Co2Al-LDH-CO3
Intensity, a.u.
0
5
10
15
20
25
30
2θ (CoKα),°

Figure 3

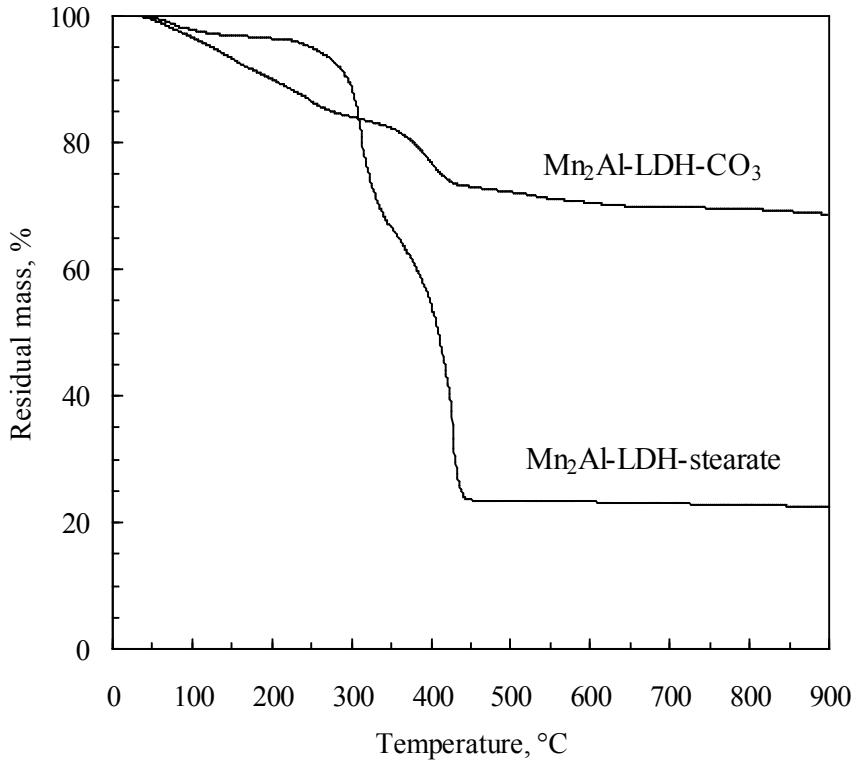
100
80
60
40
20
0
Residual mass, %
Mn2Al-LDH-CO3
Mn2Al-LDH-stearate
0
100
200
300
400
500
600
700
800
900
Temperature, °C

Figure 4

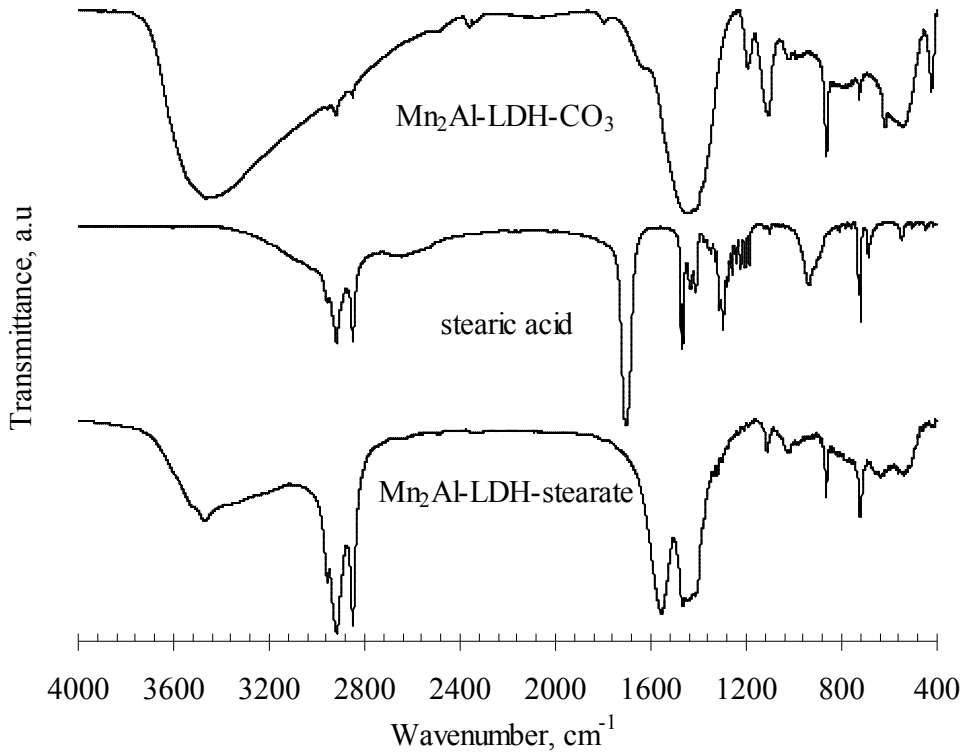
Mn2Al-LDH-CO3
stearic acid
Mn2Al-LDH-stearate
Transmittance, a.u
4000
3600
3200
2800
2400
2000
1600
1200
800
400
Wavenumber, cm-1

Figure 5

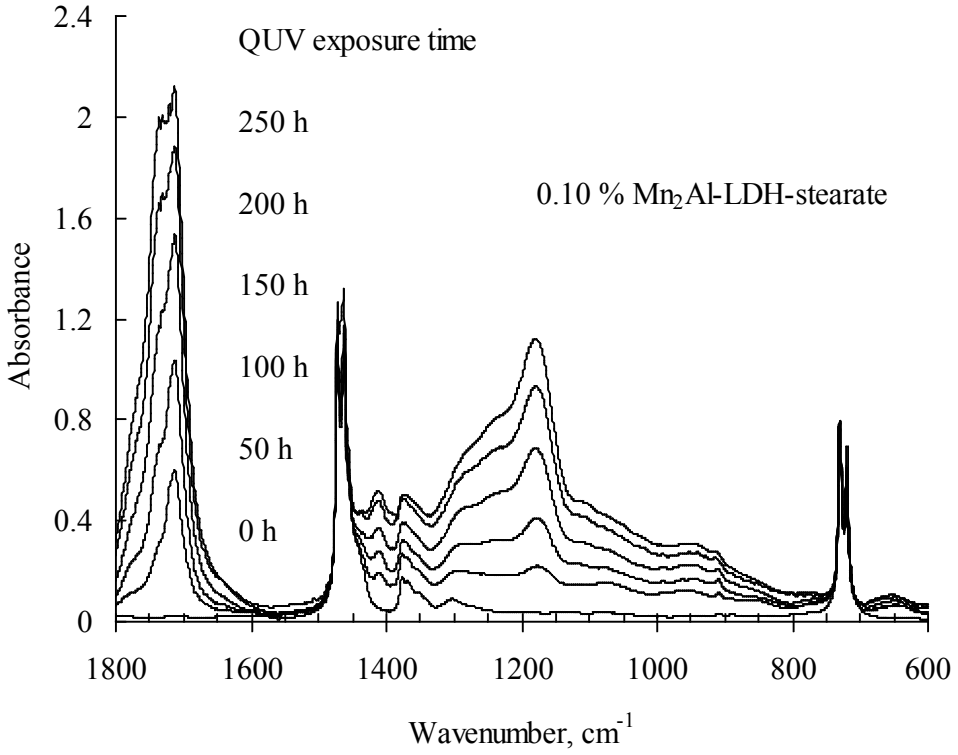
2.4
2
1.6
1.2
0.8
0.4
0
Absorbance
QUV exposure time
250 h
200 h
150 h
100 h
50 h
0 h
0.10 % Mn2Al-LDH-stearate
1800
1600
1400
1200
1000
800
600
Wavenumber, cm-1

Figure 6

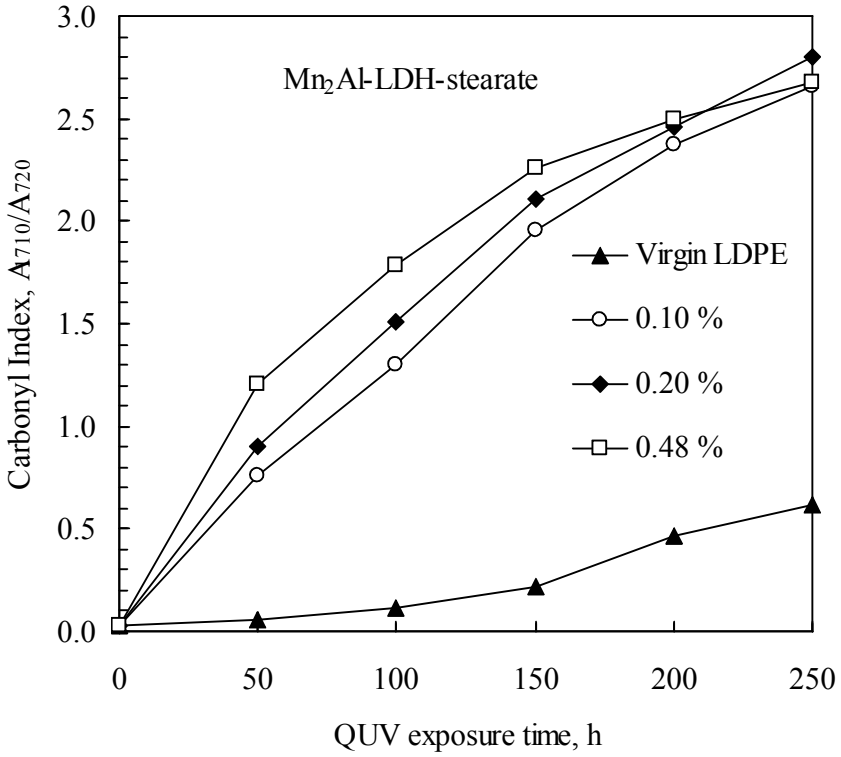
Mn2Al-LDH-stearate
Carbonyl Index, A710/A720
QUV exposure time, h
Virgin LDPE
0.10 %
0.20 %
0.48 %
0.0
0.5
1.0
1.5
2.0
2.5
3.0
0
50
100
150
200
250

Figure 7

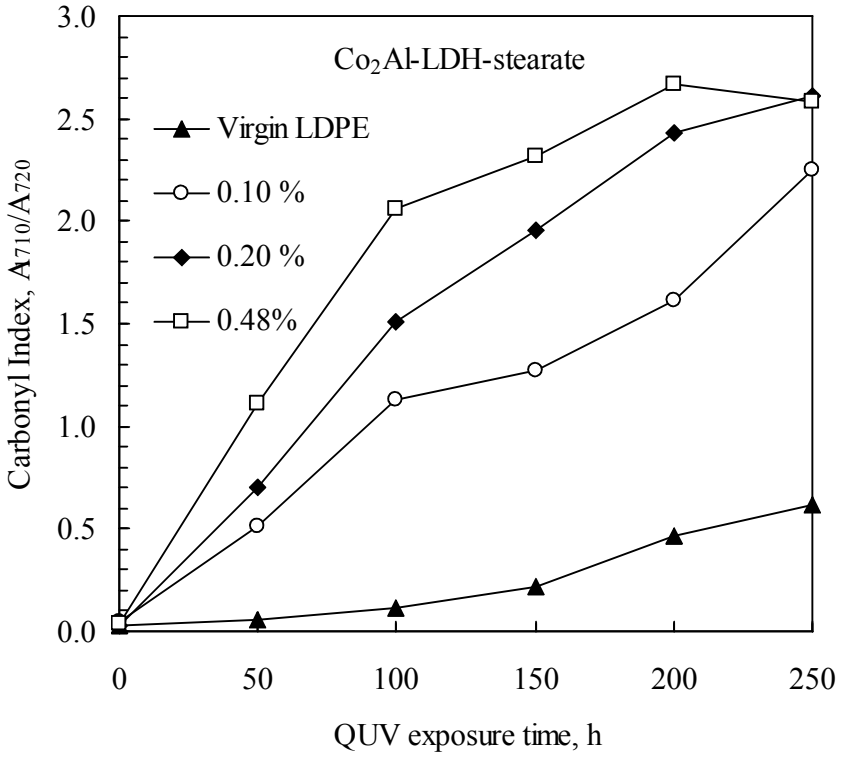
Co2Al-LDH-stearate
Virgin LDPE
0.10 %
0.20 %
0.48%
Carbonyl Index, A710/A720
QUV exposure time, h
3.0
2.5
2.0
1.5
1.0
0.5
0.0
0
50
100
150
200
250

Figure 8

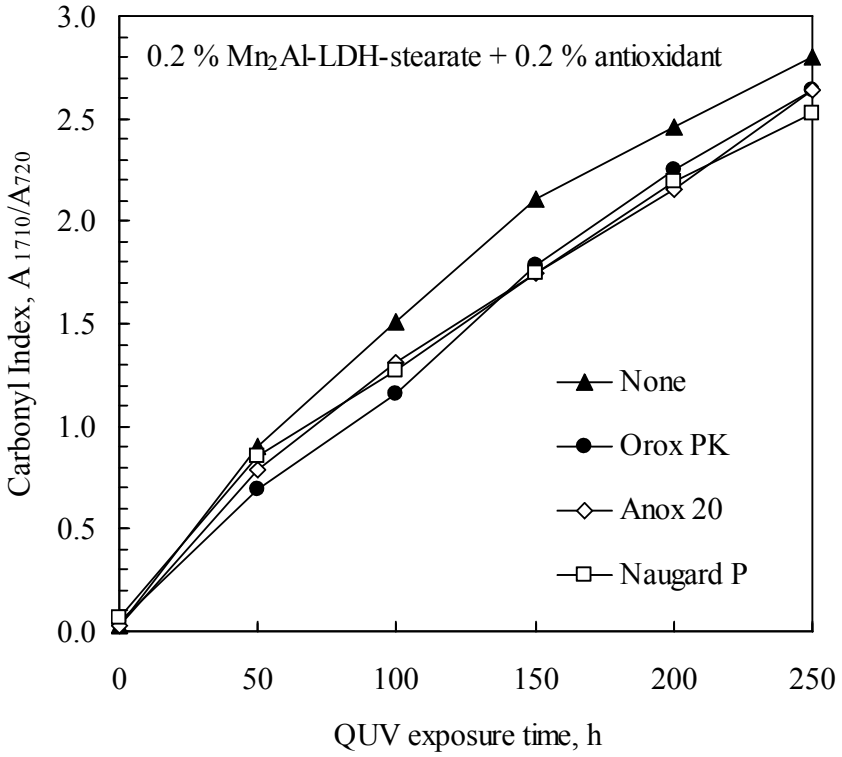
0.2 % Mn2Al-LDH-stearate + 0.2 % antioxidant
Carbonyl Index, A1710/A720
QUV exposure time, h
None
Orox PK
Anox 20
Naugard P
3.0
2.5
2.0
1.5
1.0
0.5
0.0
0
50
100
150
200
250

Figure 9

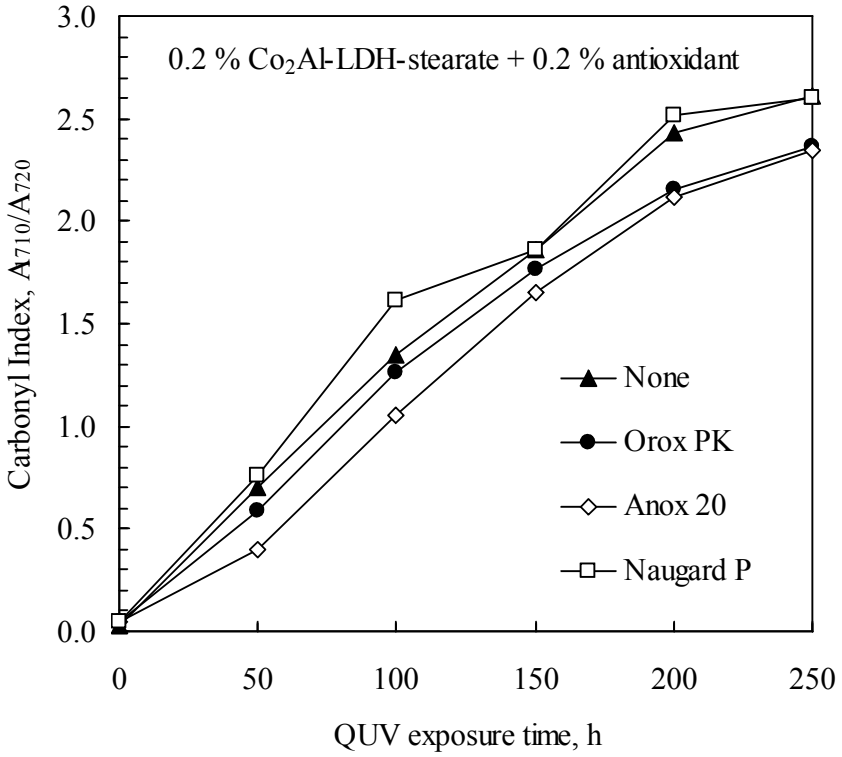
0.2 % Co2Al-LDH-stearate + 0.2 % antioxidant
Carbonyl Index, A710/A720
QUV exposure time, h
None
Orox PK
Anox 20
Naugard P
3.0
2.5
2.0
1.5
1.0
0.5
0.0
0
50
100
150
200
250

Figure 10

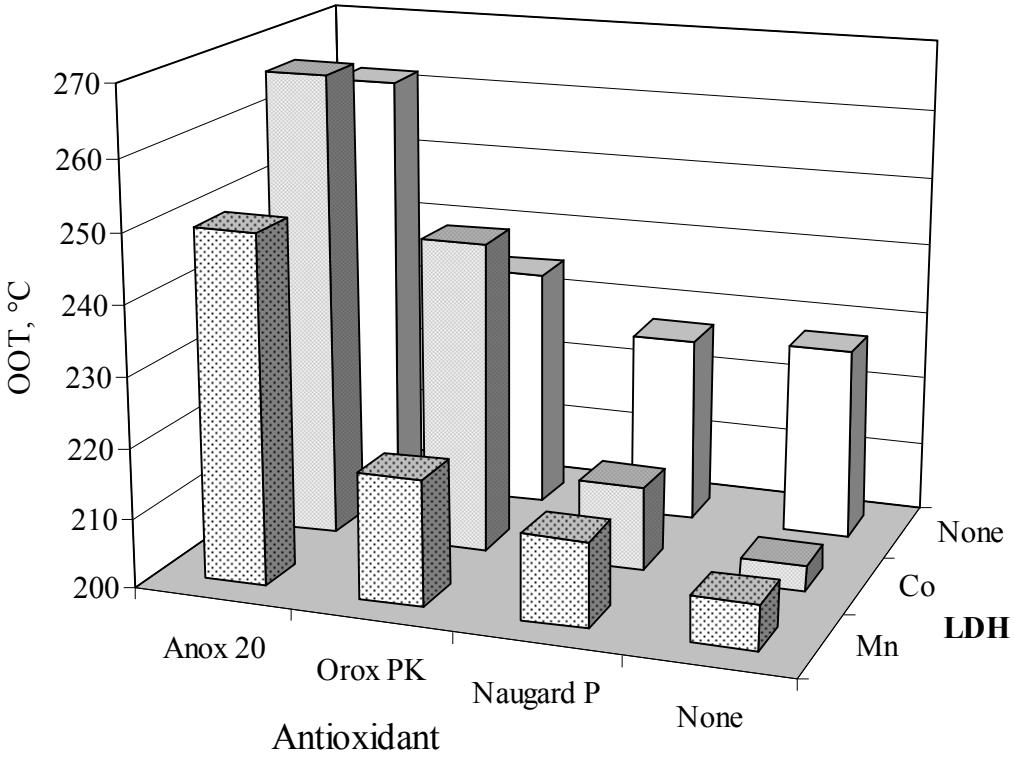
270
260
250
240
230
220
210
200
OOT, °C
Anox 20
Orox PK
Naugard P
None
Antioxidant
None
Co
Mn
LDH